ingegneria sismica
International Journal of Earthquake Engineering
Anno XLIII - Num. 1 - 2026

# Research on parking lot fire emergency response robot based on spatio-temporal adaptive risk-aware navigation algorithm

*Jianmin Lin*[1,*], *Kegang Peng*[2], *Yuanchun Li*[3], *Xin Yang*[4] *and Bin Zhang*[4]

[1] General Manager of Dayou Zhongcheng Digital Technology (Guangdong) Co., Ltd., Guangzhou, 511400, Guangdong, China
[2] Chairman of Tanda Marketing (Suqian) Co., Ltd., Suqian, 223800, Jiangsu, Chinan
[3] Xinjiang Airport (Group) Co., Ltd., Urumqi, 830000, Xinjiang, China
[4] Director of Dayou Zhongcheng Digital Technology (Guangdong) Co., Ltd., Guangzhou, 511400, Guangdong, China

**SUMMARY:** *In order to support fire emergency response in underground parking lots, this paper proposes a spatio-temporal adaptive risk-aware navigation method for fire scenes in parking lots. A computational framework integrating thermal imaging, smoke segmentation, lidar occupancy mapping, and graph search reweighting is constructed to characterize flame spread, visibility attenuation, and obstacle changes in real time. Experiments were carried out on a self-built dataset containing 12480 sets of thermal infrared-visible paired images and 3200 parking lot fire simulation scenes. The results show that the proposed method achieves 97.84% accuracy of fire target recognition, 95.31% recall rate of test set, and 34.6 ms inference delay under 320×320 input. In the path planning test, the task success rate reaches 98.6%, and the local replanning recovery delay is 0.73 s. In the two types of tasks, the global decision entropy of task A and task B is 0.912 and 0.934, respectively, and the average completion time is 23.4 s and 26.8 s, respectively, which shows that the proposed method has high stability and robustness in the parking environment with high occlusion, high thermal disturbance and dynamic blocking.*

***KEYWORDS:*** *Spatio-temporal risk perception; Fire recognition; Navigation planning; Emergency response robot*

# 1 Introduction

Underground parking lot fire has the characteristics of closed, low illumination, strong car body occlusion and fast smoke and heat diffusion. When emergency robots enter such scenes, the navigation link must not only complete target recognition and path generation, but also deal with visibility reduction, thermal damage change obstacle displacement and channel accessibility mutation. Unifying thermal imaging, visual inspection, lidar, and path planning into a computational framework has become an important research direction in public safety robotics.

In the research of mobile robot path planning, safe navigation, dynamic obstacle avoidance and real-time decision-making in complex environments are always the core contents of algorithm design. Related methods have been gradually extended from traditional heuristic search to a comprehensive modeling framework that integrates learning mechanism, multi-

*dayouzc2026@163.com
https://doi.org/10.65102/is2026270
Published: 30 April, 2026

constraint optimization and sampling expansion strategy. Wu B et al. combined smooth A with improved DWA for forklift AGV dynamic programming [1]. Yang H et al. combined enhanced DWA and improved A to enhance the global coordination in the path search process [2]. Chen Y et al. proposed a neural network navigation method to directly learn the mapping from environment state to control output [3]. Sathiya V et al. adopted fuzzy-enhanced multi-objective particle swarm optimization to realize multi-constrained path search [4]. Chen Z et al. used interval multi-objective particle swarm optimization for path planning of nuclear power inspection robot [5]. Jiang Z et al. proposed a hybrid path planning method to enhance the search ability in complex environments [6]. Liu C et al. combined PRM with D for updatable scene navigation [7]. Hao K et al. proposed the CERRT algorithm to improve the RRT scaling efficiency in complex environments [8]. Bulut V used analytical geometry and Bezier curve to improve trajectory continuity [9]. Zhang Y et al. proposed SAC-LSTM path planning method for indoor modeling [10]. Tan J combined multi-sensor fusion with deep reinforcement learning to improve the representation [11]. Li X et al. studied adaptive dynamic programming navigation and enhanced feedback correction [12]. Wang J et al. introduced multi-step backtracking experience replay for lightweight robot planning [13]. Xiao H et al. constructed a dynamic obstacle avoidance trajectory tracking method driven by reinforcement learning [14]. Tao B et al. proposed a local planning method of deep reinforcement learning to improve real-time performance [15]. Liu S et al. studied the path planning algorithm of mobile robot based on NSGA-II [16]. Wang J et al. proposed an improved RRT method to improve the performance of tree expansion and path convergence [17]. Dang T V et al. combined safe JBS-A*B and improved DWA to realize safe navigation under monocular vision conditions [18]. The above studies provide a rich technical basis for path generation of mobile robots in complex scenes. However, most of the methods are still mainly for general indoor environments, logistics scenarios or conventional dynamic obstacle conditions, and the joint modeling of smoke occlusion, thermal risk diffusion, visibility attenuation and channel security change in parking lot fire environment is still insufficient. This also provides a clear research entry point for this paper to construct a navigation method for spatio-temporal adaptive risk perception.

*Table 1: Summary of related studies*

| Research Direction | Representative Method | Core Method | Applicable Environment | Limitations Relevant to This Study |
|---|---|---|---|---|
| Dynamic path planning | Joint planning of heuristic search and local obstacle avoidance | Joint modeling of A*, DWA, PRM, RRT* and improved methods | General indoor logistics and mobile robot scenarios | Weak in characterizing smoke occlusion, heat-source diffusion, and corridor risk variation; path cost is mainly centered on distance and obstacles |
| Learning-driven navigation | Neural network and reinforcement learning navigation | Neural networks, reinforcement learning, and multi-sensor fusion navigation | Dynamic indoor environments and general mobile platforms | Strong state representation capability, but insufficient adaptation to risk transition, local distortion, and visibility attenuation in fire scenarios |
| Multi-objective optimization planning | Collaborative planning under multiple constraints | Multi-constraint planning based on particle swarm optimization, hybrid optimization, and NSGA-II | Inspection, operation, and complex constrained environments | Can handle multiple costs, but most risk terms are statically defined and lack a spatiotemporal adaptive update mechanism |
| Fire target recognition | Flame-smoke detection and spatiotemporal segmentation | Improved YOLO models, spatiotemporal attention, visual localization, and segmentation | Forest fire monitoring, video surveillance, and UAV scenarios | Strong recognition capability, but insufficient coupling with ground robot navigation, local replanning, and control decision-making |

In terms of fire perception, Mukhiddinov M et al. proposed a wildfire smoke detection system based on optimized YOLOv5 [19]. Lu K et al. studied a joint scheme of visual detection and spatial positioning [20]. Wang Z et al. proposed an improved YOLOv5 smoke detection model [21]. Shahid M et al. constructed a spatiotemporal self-attention fire detection and segmentation network [22]. Kim S Y et al. studied the forest smoke detection method based on deep learning and UAV images [23]. The existing results have a foundation in recognition accuracy and detection range. However, most of the research objects are forest fires, surveillance videos or open scenes, and the joint modeling of vehicle occlusion, low smoke layer, heat source reflection and narrow channel constraints in parking lots is still insufficient.

As shown in Fig. 1, the navigation process of the parking lot fire emergency response robot is continuously composed of five links: perception input, risk coding, traversable area determination, path generation and control execution. The sensing input receives thermal imaging images, visible light images, laser ranging data and parking lot topology information, where the fire area, smoke area, vehicle obstacles and wall boundaries are first mapped into a unified scene coordinate system. The risk coding module further combines temperature intensity, smoke diffusion speed, local visibility and channel congestion state to generate a spatio-temporal risk map, which is used to describe the dynamic risk level of different regions. The traversable area decision module screens the high-risk areas according to the risk threshold and the occupancy probability, and retains the safe connected areas for the robot to traverse. On this basis, the path generation module performs global search and local correction, so that the planning results meet the obstacle avoidance, low risk and time constraints at the same time. The control execution module then outputs steering, deceleration, detour or replanning commands according to path curvature, speed boundary and task priority, thus forming a closed-loop navigation link for fire scenarios.

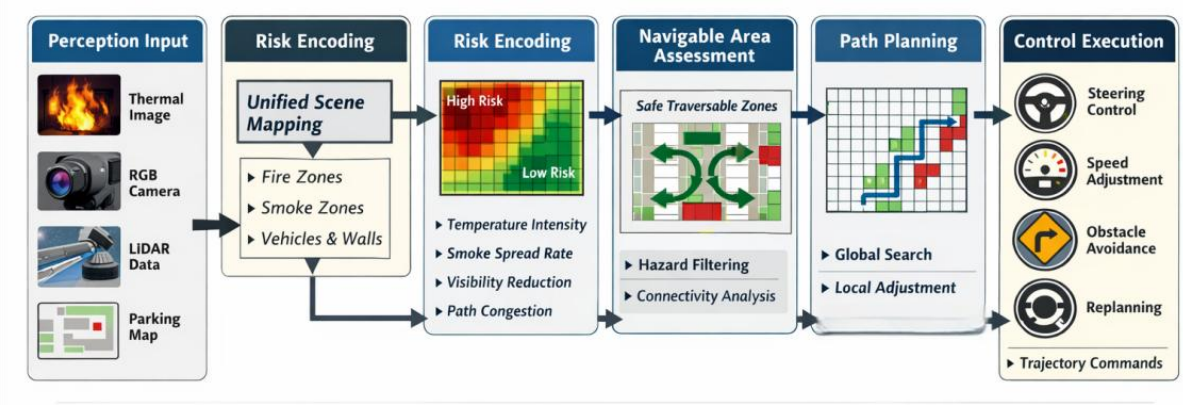


*Figure 1: Flowchart of spatio-temporal risk-aware navigation for a parking lot fire emergency response robot*

Based on the above research basis, this paper maps thermal imaging, visible light, laser ranging and topological constraints into a unified spatio-temporal risk map, and constructs an integrated method for fire target recognition, risk-aware navigation and control decision for fire scenes in parking lots. The verification will be carried out around the recognition accuracy, recall rate, reasoning delay, path length, replanning time, collision rate and global decision entropy to support autonomous reconnaissance and response in closed fire environment.

# 2 Methods and materials

## 2.1 Kinematics analysis and spatio-temporal scene modeling of parking lot fire emergency response robot

The fire scene in parking lots has the characteristics of closed space, dense parking Spaces, variable smoke and heat diffusion, and rapid attenuation of visibility. When the robot performs reconnaissance, guidance and material delivery tasks, motion control and scene modeling must be completed simultaneously. In order to ensure that the subsequent fire recognition, risk coding and navigation planning are established on the basis of unified computing, this section first models the kinematic constraints and spatio-temporal scene expression of the parking lot fire emergency response robot.

In this paper, the two-wheel differential chassis is selected as the mobile carrier, the front end of the vehicle body is integrated with a thermal infrared camera, a visible light camera, a two-dimensional laser radar, an inertial measurement unit and a gas concentration sensor, and the rear end is equipped with a calculation and communication module. The differential chassis has compact structure and small steering radius, which is suitable for maneuvering tasks in narrow passages between parking trains. The robot receives the environment sensing data and maps the flame area, smoke area, vehicle contour and wall boundary into the coordinate system. The system structure is shown in Fig. 2.

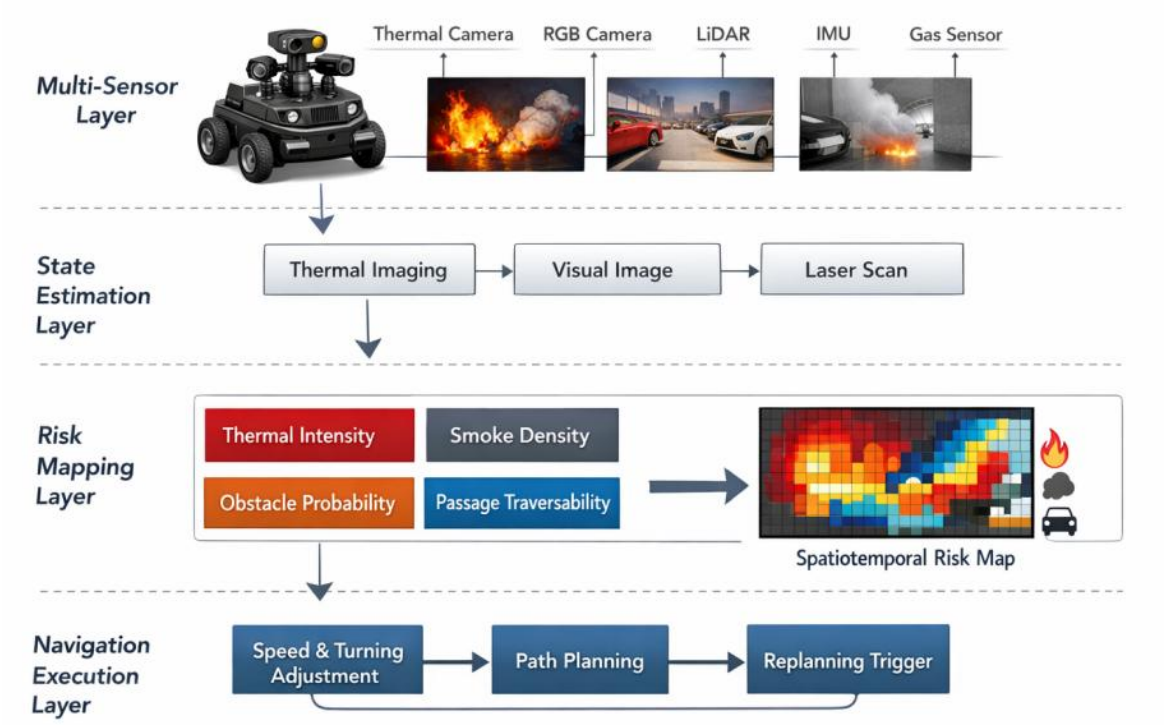


*Figure 2: Structural diagram of kinematics and spatio-temporal scene modeling for a fire emergency response robot in a parking lot*

As shown in Fig. 2, the structure is mainly divided into multi-source perception layer, state estimation layer, risk mapping layer and navigation execution layer. The multi-source perception layer is responsible for collecting thermal radiation, image texture and distance information. The state estimation layer completed the pose calculation and error correction. The risk mapping layer generates spatio-temporal risk maps according to thermal field intensity,

smoke layer thickness, obstacle occupancy probability and channel traffic degree. The navigation execution layer adjusts the speed, rotation Angle and replanning trigger conditions according to local risk changes.

In order to describe the plane motion relationship of the robot, this paper uses the discrete time difference model to describe the position and orientation update of the vehicle body, and its mathematical expression is shown in Formula (1).

$$\begin{bmatrix} x_{t+1} \\ y_{t+1} \\ \theta_{t+1} \end{bmatrix} = \begin{bmatrix} x_t + \dfrac{v_r^t + v_l^t}{2} \cos\theta_t \ \Delta t \\ y_t + \dfrac{v_r^t + v_l^t}{2} \sin\theta_t \ \Delta t \\ \theta_t + \dfrac{v_r^t - v_l^t}{b} \Delta t \end{bmatrix} \tag{1}$$

where $x_t$ and $y_t$ represent the position of the robot in the global coordinate system at time $t$, $\theta_t$ represents the heading Angle, $v_r^t$ and $v_l^t$ represent the linear velocity of the right wheel and the left wheel respectively,$\Delta t$ represents the control period, and $b$ represents the distance between the centers of the two driving wheels. This equation directly maps the actuation instructions to pose increments.

The adhesion coefficient of parking lot ground will fluctuate under the influence of high temperature water spray and debris scattering, and it is difficult to reflect the real motion deviation by simply relying on the ideal differential model. Therefore, this paper introduces the state transition equation with disturbance term to modify the velocity propagation, and its mathematical expression is shown in Eq. (2).

$$s_{t+1} = A_t s_t + B_t u_t + \Gamma_t \xi_t, \quad A_t = \begin{bmatrix} 1 & 0 & -v_t \Delta t \sin\theta_t & \Delta t \cos\theta_t & 0 \\ 0 & 1 & v_t \Delta t \cos\theta_t & \Delta t \sin\theta_t & 0 \\ 0 & 0 & 1 & 0 & \Delta t \\ 0 & 0 & 0 & 1 & 0 \\ 0 & 0 & 0 & 0 & 1 \end{bmatrix} \tag{2}$$

where, $s_t$ represents the state vector composed of position, heading, velocity and angular velocity, $u_t$ represents the control vector composed of left and right wheel angular velocity and braking command, $A_t$ and $B_t$ represent the state transition matrix and control input matrix respectively, $\Gamma_t$ represents the disturbance mapping matrix, $\xi_t$ represents the random noise formed by the wet and smoke flow disturbance. This formula is able to estimate the motion offset recursively.

After completing the kinematic modeling, it is still necessary to translate the thermal hazard intensity, smoke density, and obstacle occupancy relationships into computable risk expressions. In this paper, a grid spatio-temporal risk field is constructed, and the unit risk value is generated by multi-source weighting, whose mathematical expression is shown in Formula (3).

$$R_t(p) = \alpha H_t(p) + \beta S_t(p) + \gamma O_t(p) + \delta C_t(p) + \eta \sum_{\tau=t-k}^{t} \lambda^{t-\tau} D_\tau(p) \tag{3}$$

Here, $R_t(p)$ represents the comprehensive risk value at position $p$ at time $t$, $H_t(p)$ represents the thermal intensity component, $S_t(p)$ represents the smoke occlusion component, $O_t(p$ represents the obstacle occupation component, $C_t(p)$ represents the channel congestion component, $D_\tau(p)$ represents the risk residual term at historical time, $\alpha$, $\beta$, $\gamma$, $\delta$ and $\eta$ are

the weight coefficients. Let $\lambda$ be the time decay factor. This formula takes the instantaneous sensing result and the short-term historical evolution into the same cost space.

Risk alone is still not enough to support path search, because the actual movement of the robot depends on the traversability cost between neighboring nodes. To this end, this paper further constructs the edge weight model of the scene graph, and encodes the distance, curvature and risk gradient into the edge connection together, whose mathematical expression is shown in Equation (4).

$$w_{ij} = \|p_i - p_j\|_2\left(1 + \mu\bar{R}_{ij}^2 + \nu|\Delta\theta_{ij}|\right) + \frac{\rho}{V_{ij} + \varepsilon} \tag{4}$$

Here, $w_{ij}$ represents the edge weight cost from node $i$ to node $j$, $\|p_i - p_j\|_2$ represents the Euclidean distance between nodes, $\bar{R}_{ij}^2$ represents the average risk intensity on the path segment, $\Delta\theta_{ij}$ represents the heading change, $V_{ij}$ represents the effective visibility of the corresponding channel, $\mu$, $\nu$ and $\rho$ are the regulation coefficients, and $\varepsilon$ is the minimal constant to prevent the denominator from being zero. This formula makes the search process not only pursue the shortest distance, but also suppress the sharp change path, the high-risk path and the low visibility path.

Based on the above kinematic constraints, state propagation relationship, spatio-temporal risk field expression and edge weight cost construction, the basic computational model of the parking lot fire emergency response robot can be unified. On the one hand, the model provides a continuous state support for robot pose estimation in narrow parking passages, occlusion environments and low visibility conditions. On the other hand, it also compreszes heat hazards, smoke, obstacles and traffic changes into a computable risk space. The subsequent fire target recognition, risk-aware path planning and navigation decision control can be established on the consistent coordinate representation and cost expression. The resulting kinematics and scene modeling results provide a direct data basis and constraint basis for the generation of spatio-temporal adaptive risk coding and navigation strategy.

## 2.2 Fire target recognition method based on spatio-temporal adaptive risk coding

After the kinematic analysis and spatio-temporal scene modeling are completed, the fire target recognition module can calculate in coordinates. The fire image of parking lot is affected by low illumination, smoke occlusion, vehicle body reflection, heat source and target scale change at the same time, and the detection network is prone to miss detection of small flames, boundary drift of smoke masses and misjudgment of heat spots. In order to ensure stable input for subsequent risk mapping and navigation planning, a fire target recognition method based on spatio-temporal adaptive risk coding is constructed in this section. The method takes visible light images, thermal infrared images and sequence information as input, extracts texture, temperature and time series features in the backbone network, and introduces a risk coding unit in the fusion stage, so that the model considers spatial context and time relationship synchronously when detecting fire, smoke and dangerous areas.

The recognition network in this study consists of a bimodal input layer, a backbone feature extraction layer, a spatio-temporal risk coding layer, a multi-scale fusion layer, and a detection output layer. The visible light branch is responsible for preserving the edge, contour and occlusion relationship, and the thermal infrared branch is responsible for highlighting the high temperature area and the thermal diffusion direction. The two branches are aligned in the middle layer. In order to avoid local information suppression caused by fixed-weight fusion, this paper

introduces spatio-temporal adaptive risk coding after feature alignment, and writes temperature gradient, smoke concentration and historical frame changes into the feature map weights. The structure is shown in Fig. 3.

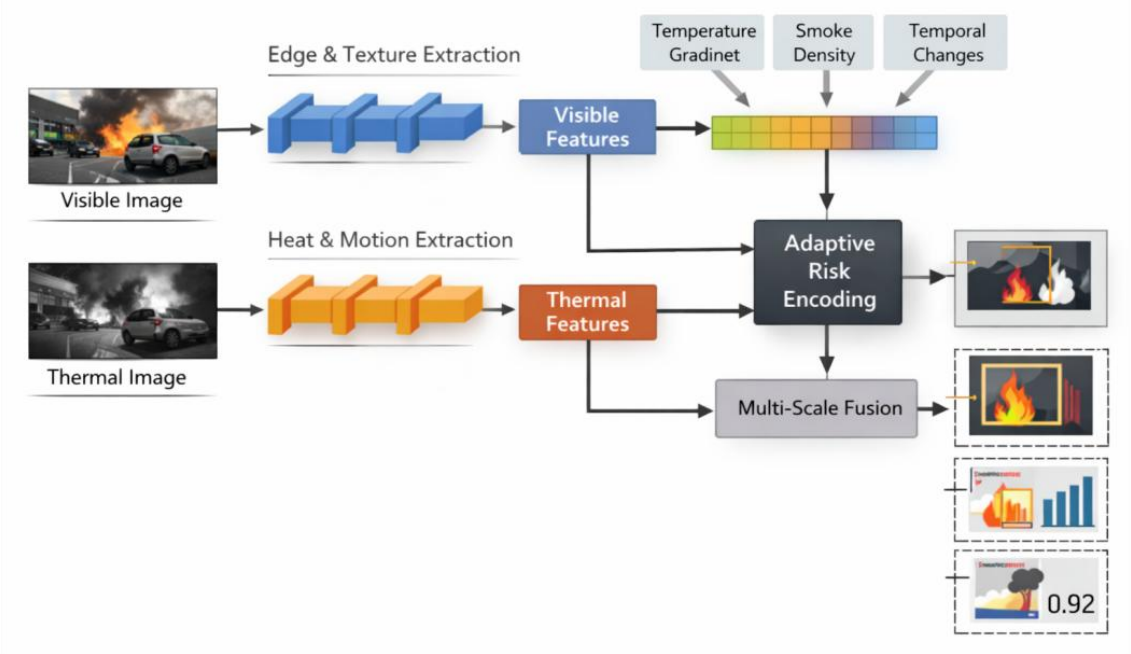


*Figure 3: Structure diagram of fire target recognition method based on spatio-temporal adaptive risk coding*

As shown in Fig. 3, the visible light feature tensor and the thermal infrared feature tensor of the input image are formed after the dual-branch convolution coding, and then enter the risk coding module. Instead of directly classifying the original image, the module reweights the feature responses so that flame edges, smoke wakes, and dangerous hot areas achieve high expression intensity in the fusion stage. After the risk weighting is completed, the network outputs the target category, confidence and bounding box position on the multi-scale detection head, so as to provide fire input for the subsequent planning module.

In order to depict the fusion features after risk coding, spatial features, temporal features and thermal information are jointly mapped into an enhanced representation, whose mathematical expression is shown in Equation (5).

$$F_t^r = \sigma\left(W_v F_t^v + W_i F_t^i + W_m M_t + W_d \Delta F_t + b\right) \odot \left(F_t^v \oplus F_t^i\right) \tag{5}$$

where $F_t^r$ represents the risk coding fusion feature at time $t$, $F_t^v$ and $F_t^i$ represent the intermediate features of the visible and thermal infrared branches respectively, $M_t$ represents the risk map composed of smoke concentration, temperature gradient and occlusion probability, $\Delta F_t$ represents the feature difference between adjacent frames, $W_v$, $W_i$, $W_m$ and $W_d$ are learnable weight matrices, and $b$ is the bias term. $\sigma(\cdot)$ is the activation function, $\odot$ is element-wise multiplication, and $\oplus$ is feature concatenation. This formula compresses bimodal observations, scene risk and temporal variation into the same feature space.

In the target box regression stage, the ordinary intersection over union loss is difficult to reflect the positioning deviation caused by the irregular boundary between the smoke envelope and the flame. To this end, this paper constructs the composite regression loss with risk modulation term, whose mathematical expression is shown in Equation (6).

$$L_{reg} = 1 - IoU(B_p, B_g) + \frac{\rho^2(c_p, c_g)}{d^2 + \varepsilon} + \lambda\left(1 - \cos(\theta_p - \theta_g)\right) + \mu\bar{R}(B_p) \quad (6)$$

Here, $L_{reg}$ represents the regression loss of the target box, $B_p$ and $B_g$ represent the intersection and union ratio between the predicted box and the true box, $IoU(B_p, B_g)$ represents the square of the Euclidean distance between the two, $\rho^2(c_p, c_g)$ represents the square of the Euclidean distance between the center point, $d^2$ represents the diagonal length of the minimum bounding box, $\varepsilon$ is the minimum constant, and $\theta_p$ and $\theta_g$ represent the main direction Angle between the predicted box and the true box. $\bar{R}(B_p)$ represents the average risk value in the coverage area of the prediction box, and $\lambda$ and $\mu$ are the regulation coefficients. In addition to the position error, this equation further constrains the orientation consistency and the positioning deviation of the high-risk area.

In the stage of classification and confidence calculation, this paper uses a risk-guided joint scoring mechanism to screen the candidate boxes, whose mathematical expression is shown in Equation (7).

$$S_k = P_k^c \cdot P_k^o \cdot \exp(-\gamma R_k) \cdot (1 + \alpha T_k + \beta Q_k) \quad (7)$$

where, $S_k$ represents the final score of the $k$ candidate target, $P_k^c$ represents the class probability, $P_k^o$ represents the probability of target existence, $R_k$ represents the average risk intensity of the candidate region, $T_k$ represents the temperature significance response given by the thermal infrared branch, $Q_k$ represents the stability factor calculated from the time series consistency, $\alpha$, $\beta$, $\gamma$ are the weight coefficients. This equation is able to suppress the pseudo-high response caused by metal reflection and local thermal spots, while retaining the continuously expanding flame and smoke targets.

Based on the above design, the training process of the target recognition module includes data labeling, dual-modal synchronization enhancement, backbone network pre-training, joint optimization of risk coding and convergence of detection head parameters. In the inference stage, the model first completed the bimodal feature extraction, then calculated the risk coding map, and finally output the flame box, smoke box and dangerous hot area box. The recognition result not only retains the target category and location, but also gives the structured intensity information that can be directly written into the spatio-temporal risk map, which provides a continuous, stable and computable fire input basis for subsequent risk-aware navigation path planning and navigation control strategy.

## 2.3 Risk-aware navigation path planning method in uncertain fire environment of parking lot

After the construction of the fire target recognition method, the robot has been able to obtain the structured output of flame area, smoke area, high temperature area and passable boundary. In order for a robot to reach a specified position in a parking lot fire environment, local obstacle avoidance relying only on instantaneous sensing feedback is still not sufficient to support continuous navigation. There are uncertain factors in the parking lot, such as vehicle occlusion, smoke layer flow, local collapse and heat source diffusion, so the path planning process needs to deal with spatial connectivity, time variability and risk gradient simultaneously. Based on this, this paper constructs a risk-aware navigation path planning method for uncertain conditions. The risk bias mechanism is introduced in the sampling expansion stage, the safety cost re-ranking is introduced in the parent node selection stage, and the time consistency check

and curvature smoothing are added after the path generation, so that the planning result satisfies the accessibility, safety and motion executability at the same time.

The core process of the proposed method consists of four parts: risk-guided sampling, constraint expansion connection, candidate path reranking and trajectory smoothing. In the initial stage, the robot takes the current position as the root node and searches synchronously on the local traversable graph and the global topology graph. Different from ordinary random sampling, this paper does not sample in the global space with equal probability, but adjusts the sampling probability according to the risk distribution output by the fire recognition module, so that the low risk and strongly connected area can obtain higher sampling density. To describe this process, this paper defines the risk-biased sampling probability, whose mathematical expression is shown in Equation (8).

$$P(x) = \frac{\exp[-\alpha R(x)] \cdot (1 + \beta G(x)) \cdot (1 + \kappa T(x))}{\int_{\Omega} \exp[-\alpha R(\xi)] \cdot (1 + \beta G(\xi)) \cdot (1 + \kappa T(\xi))\, d\xi} \tag{8}$$

Here, $P(x))$ represents the probability of location $x$ being selected as a sampling point, $R(x)$ represents the comprehensive risk intensity of the location, $G(x)$ represents the topological connectivity response, $T(x)$ represents the channel traffic trend factor, $\Omega$ represents the searchable space, and $\alpha$, $\beta$ and $\kappa$ are the regulation coefficients. This formula transforms the sampling process from uniform expansion to adaptive expansion with risk bias, which can reduce the invalid exploration of high-risk areas.

Here, P(x) represents the probability of location x being selected as a sampling point, R(x) represents the comprehensive risk intensity of the location, G(x) represents the topological connectivity response, T(x) represents the channel traffic trend factor, Ω represents the searchable space, and α, β and κ are the regulation coefficients. This formula transforms the sampling process from uniform expansion to adaptive expansion with risk bias, which can reduce the invalid exploration of high-risk areas.

After completing the sampling, the tree structure needs to select the optimal parent from the neighborhood nodes. The common RRT usually completes the connection only based on the geometric distance, which is easy to obtain the path through the smoke accumulation area or narrow heat passage in the fire environment. In this paper, the comprehensive connection cost is constructed in the parent node selection stage, and the path length, risk gradient, minimum safe distance and direction mutation are uniformly encoded. Its mathematical expression is given in Equation (9).

$$J_{i\to j} = d_{ij} + \lambda_1 \int_0^1 R\left(\phi_{ij}(s)\right) ds + \lambda_2 \max_{s\in[0,1]} \left\|\nabla R\left(\phi_{ij}(s)\right)\right\| + \lambda_3 \frac{1}{c_{ij} + \varepsilon} + \lambda_4 \left|\theta_j - \theta_i\right| \tag{9}$$

Here, $J_{i\to j}$ represents the comprehensive cost of connecting node $i$ to node $j$, $d_{ij}$ represents the Euclidean distance between the two nodes, $\phi_{ij}(s)$ represents the parameterized trajectory on the connecting line segment, $R(\cdot)$ represents the risk value on the trajectory, $\nabla R(\cdot)$ represents the risk gradient, $c_{ij}$ represents the minimum safe distance of the path segment, and $\theta_i$ and $\theta_j$ represent the heading Angle corresponding to the node. $\lambda_1$ to $\lambda_4$ are the weight coefficients and $\varepsilon$ is a minimal constant. This formula makes the parent node selection not only rely on the shortest connection, but give priority to retaining the expansion path with lower risk, smoother boundary and higher passability margin.

The parking lot fire environment has obvious temporal disturbance characteristics, and the availability of the same path at different moments may change. In order to avoid the rapid failure of the path after generation, this paper further introduces the temporal consistency check, which

evaluates the dynamic feasibility of each segment on the candidate path. Its mathematical expression is given in Equation (10).

$$Q(\pi) = \prod_{m=1}^{M} \mathbb{I}\left(\tau_m < \tau_m^{max}\right) \cdot \exp\left[-\sum_{m=1}^{M} \left(\mu_1 \bar{R}_m + \mu_2 \bar{S}_m + \mu_3 \bar{H}_m\right) \Delta t_m\right] \tag{10}$$

where $Q(\pi)$ represents the time consistency score of the candidate path $\pi$, $M$ represents the number of segments after the path is decomposed, $\mathbb{I}(\cdot)$ is the indicator function,$\tau_m$ represents the expected passage time of the $m$ segment,$\tau_m^{max}$ represents the maximum safe passage time allowed in this segment, $\bar{R}_m$, $\bar{S}_m$ and $\bar{H}_m$ represent the average risk value, average smoke occlusion intensity and heat equalization damage intensity on this segment, respectively. $\Delta t_m$ shows the time consumption of passing through this segment, and $\mu_1$, $\mu_2$, and $\mu_3$ are the adjustment parameters. This formula can filter the short-term stability of the path, so that the final retained candidate results have stronger continuous executability.

After path selection, the discrete node connection may still appear sharp turning and local jitter, which is not conducive to the continuous operation of the differential chassis on the slippery ground and narrow lane. To this end, in this paper, the optimal discrete path is smoothed with curvature constraints and a quintic parameterized trajectory is used to generate the final control reference line. Its mathematical expression is given in Equation (11).

$$\Gamma(u) = \sum_{n=0}^{5} B_n^5(u) P_n, \quad B_n^5(u) = \binom{5}{n} u^n (1-u)^{5-n},$$

$$\mathcal{C}(\Gamma) = \int_0^1 \left(\omega_1 \|\Gamma'(u)\|^2 + \omega_2 \|\Gamma''(u)\|^2 + \omega_3 \max(0, \kappa(u) - \kappa_{max})^2\right) du \tag{11}$$

Here, $\Gamma(u)$ represents the smoothed parameterized trajectory, $P_n$ represents the control points, $B_n^5(u)$ represents the quintuple basis functions, $\mathcal{C}(\Gamma)$ represents the trajectory smoothing cost, $\Gamma'(u)$ and $\Gamma''(u)$ represent the first and second derivatives of the trajectory, $\kappa(u)$ represents the local curvature, $\kappa_{max}$ represents the maximum curvature allowed by the robot. $\omega_1$, $\omega_2$ and $\omega_3$ are the weight coefficients. This equation suppresses local high curvature and frequent turns while keeping the path passing through critical nodes, so that the output trajectory is more in line with the actual execution constraints.

Based on the above design, the risk-aware navigation path planning method in this paper completes the tree expansion with risk bias in the search phase, the comprehensive safety cost screening in the connection phase, the temporal consistency check in the evaluation phase, and the curvature limited smoothing in the output phase. The generated planning result is no longer limited to the shortest path, but forms an executable path taking into account the dynamic disturbance of fire, local safety margin and the continuity of robot motion, which provides a stable input for the subsequent navigation decision and control strategy design.

## 2.4 Navigation decision and control strategy design of parking lot fire emergency response robot

After the design of the above fire target recognition method and risk-aware path planning method, the robot has been able to obtain the flame location, smoke diffusion area, dangerous hot area and candidate passage path. In order to assist robots to complete tasks such as inspection, approach, avoidance, guidance and evacuation in the fire environment of parking

lots, it is also necessary to form an executable navigation decision and control strategy based on the path. Due to the fluctuation of visibility, local high temperature, vehicle occlusion and temporary obstacle changes inside the parking lot, the robot cannot only rely on the static path during the movement, but needs to dynamically adjust its behavior according to the state changes. Based on this, this paper uses the hierarchical state decision method to complete the navigation control modeling, and constructs the control strategy of the robot in different task stages by the statechart driven way.

In the process of control modeling, this paper divides the main behaviors of the parking lot fire emergency response robot in the execution process into five types of states, which are standby monitoring, fire approach, safe detour, task execution and path evacuation. The input information, control target and action output in different states are not the same, so it is necessary to describe the relationship between the state set, the event set and the control output. To this end, this paper first constructs the navigation decision state model, whose mathematical expression is shown in Equation (12).

$$\mathcal{D} = (\mathcal{S}, \mathcal{E}, \mathcal{U}, \mathcal{F}, \mathcal{Y}) \tag{12}$$

where $\mathcal{D}$ represents the navigation decision model, $\mathcal{S}$ represents the state set, including five states of standby monitoring, fire approach, safe detour, task execution and path evacuation, $\mathcal{E}$ represents the event set, which is used to describe the trigger conditions such as flame recognition, smoke enhancement, path blocking, target arrival and evacuation completion, $\mathcal{U}$ represents the control input set, $\mathcal{F}$ represents the state transition function. $\mathcal{Y}$ denotes the set of control outputs. This formula provides the formal basis of the whole navigation decision strategy.

On this basis, the system needs to complete the state switch according to the sensing result and the execution state. Different from the fixed rule switching, the state change in the fire environment is affected by the risk intensity, the remaining path length, the task priority and the path stability. To this end, this paper defines the state transition probability with risk constraint, whose mathematical expression is shown in Equation (13).

$$\mathrm{P}(\mathrm{s}_{\mathrm{t+1}} = \mathrm{j} \mid \mathrm{s}_{\mathrm{t}} = \mathrm{i}) = \frac{\exp\left[-\alpha \bar{\mathrm{R}}_{\mathrm{ij}} - \beta \mathrm{L}_{\mathrm{ij}} + \gamma \mathrm{U}_{\mathrm{j}} + \delta \mathrm{C}_{\mathrm{ij}}\right]}{\sum_{\mathrm{k} \in \mathcal{N}(\mathrm{i})} \exp[-\alpha \bar{\mathrm{R}}_{\mathrm{ik}} - \beta \mathrm{L}_{\mathrm{ik}} + \gamma \mathrm{U}_{\mathrm{k}} + \delta \mathrm{C}_{\mathrm{ik}}]} \tag{13}$$

where,$\mathrm{P}(\mathrm{s}_{\mathrm{t+1}} = \mathrm{j} \mid \mathrm{s}_{\mathrm{t}} = \mathrm{i})$ represents the probability of the robot to transition from state $\mathrm{i}$ to state $\mathrm{j}$ at time $\mathrm{t}$, $\bar{\mathrm{R}}_{\mathrm{ij}}$ represents the average risk value of the path segment corresponding to state transition, $\mathrm{L}_{\mathrm{ij}}$ represents the remaining path length to the goal state,$\mathrm{U}_{\mathrm{j}}$ represents the task urgency of state $\mathrm{j}$, $\mathrm{C}_{\mathrm{ij}}$ represents the control executability score. $\mathcal{N}(\mathrm{i})$ denotes the set of candidate successors of state $\mathrm{i}$, and $\alpha$, $\beta$, $\gamma$ and $\delta$ are the regulation coefficients. This formula allows state transitions to take into account risk, safety, and task prioritization, rather than being triggered by a single event.

In order to transform the path planning output into the control target directly, the navigation reference point is defined in the local coordinate system and mapped into the global coordinate system according to the current position and orientation of the robot. This process facilitates smooth steering and short-time replanning in narrow passages and near the edge of obstacles. The mathematical expression of the coordinate transformation of the reference point is shown in Eq. (14).

$$\begin{bmatrix} \mathrm{x}_{\mathrm{g}} \\ \mathrm{y}_{\mathrm{g}} \end{bmatrix} = \begin{bmatrix} \mathrm{x}_{\mathrm{r}} \\ \mathrm{y}_{\mathrm{r}} \end{bmatrix} + \begin{bmatrix} \cos\theta_{\mathrm{r}} & -\sin\theta_{\mathrm{r}} \\ \sin\theta_{\mathrm{r}} & \cos\theta_{\mathrm{r}} \end{bmatrix} \begin{bmatrix} \mathrm{x}_{\mathrm{l}} \\ \mathrm{y}_{\mathrm{l}} \end{bmatrix} + \begin{bmatrix} \zeta_{\mathrm{x}} \\ \zeta_{\mathrm{y}} \end{bmatrix} \tag{14}$$

where, $(x_g, y_g)$ represents the navigation reference point in the global coordinate system, $(x_r, y_r)$ represents the current position of the robot, $\theta_r$ represents the current heading Angle of the robot, $(x_l, y_l)$ represents the preview point or steering reference point in the local coordinate system, and $(\zeta_x, \zeta_y)$ represents the position correction term caused by ground slip, smoke flow disturbance and sensing error. This formula completes the real-time projection of the local path point to the control target point.

In the control allocation phase, only giving the target point is still not enough to support continuous execution in complex environments, and it is also necessary to write the position error, heading error and risk suppression into the control law together. To this end, this paper defines the speed control output under risk suppression, whose mathematical expression is shown in Equation (15).

$$\begin{aligned} v_t &= v_{\max} \tanh(k_1 e_d) \exp(-\lambda_1 R_t - \lambda_2 S_t) \\ \omega_t &= k_2 e_\theta + k_3 \int_0^t e_\theta(\tau)\, d\tau + k_4 \frac{de_\theta}{dt} - \lambda_3 \nabla R_t \end{aligned} \tag{15}$$

Here, $v_t$ represents the linear velocity output, $\omega_t$ represents the angular velocity output, $v_{max}$ represents the maximum allowed linear velocity, $e_d$ represents the distance error between the robot and the reference point, $e_\theta$ represents the heading error, $R_t$ represents the risk intensity of the current position, $S_t$ represents the smoke occlusion intensity, $\nabla R_t$ represents the local risk gradient, and $k_1$ to $k_4$ is the control gain. $\lambda_1$, $\lambda_2$, and $\lambda_3$ are the risk suppression coefficients. This formula ensures that the robot maintains high mobility in the low risk area, and automatically reduces the speed and corrects the steering in the high risk area.

As shown in Fig. 4, the navigation decision and control strategy is mainly divided into four parts: state perception, state selection, control allocation and action correction. The state perception part receives the output of the fire recognition module and the path planning module. The state selection part determines the current task phase according to the state transition rules. The control allocation part generates velocity, angular velocity and replanning markers according to different states. The action correction part compensates the control quantity combined with the real-time error.

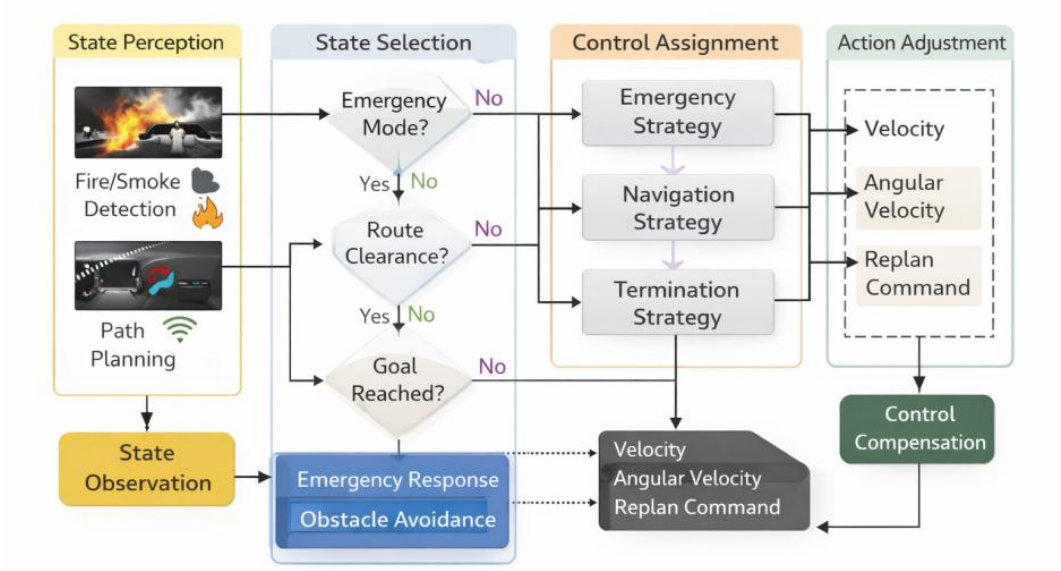


*Figure 4: Flow chart of navigation decision and control strategy for a fire emergency response robot in a parking lot*

In addition, obstacles and heat sources in the fire environment of the parking lot may change the original path effectiveness in a short time, so the control layer also needs to judge when to trigger local replanning. In order to avoid control jitter caused by frequent switching, this paper constructs a replanning trigger decision function, whose mathematical expression is shown in Equation (16).

$$\Psi_t = \mathbb{I}(R_t > R_{\text{th}}) \vee \mathbb{I}(d_{\text{obs}} < d_{\min}) \vee \mathbb{I}(Q_t < Q_{\min}) \vee \mathbb{I}(|e_\theta| > \theta_{\max}) \tag{16}$$

Here, $\Psi_t$ represents the replanning trigger flag at time t, $\mathbb{I}(\cdot)$ is the indicator function, $R_t$ represents the local risk intensity, $R_{\text{th}}$ represents the risk threshold, $d_{\text{obs}}$ represents the distance from the robot to the nearest obstacle, $d_{\min}$ represents the minimum safe distance, $Q_t$ represents the time consistency score of the current path, $Q_{\min}$ represents the minimum consistency threshold allowed. Let $\theta_{\max}$ denote the maximum acceptable heading error. This formula enables local replanning to be triggered only under necessary conditions, thus maintaining the continuity of the execution process.

Based on the above design, the navigation decision and control strategy constructed in this paper realizes a unified closed loop of state modeling, state transition, reference point transformation, speed control and replanning trigger. The strategy can convert the fire information output by the recognition module and the candidate path generated by the planning module into executable control commands, and maintain high decision stability under the conditions of enhanced smoke occlusion, sudden change of risk gradient and local channel block. The control link thus formed provides direct support for the autonomous approach, avoidance detour and task evacuation of fire emergency response robots in parking lots in complex and uncertain environments.

# 3 Results

## 3.1 Performance analysis of fire target recognition method based on spatio-temporal adaptive risk coding

In order to verify the applicability of the fire target recognition method based on spatio-temporal adaptive risk coding in the parking lot fire scene, the experiment was trained and tested in Ubuntu 22.04, PyTorch 2.1 and CUDA 12.1 environments, and the converged model was deployed to the inference framework of the robot side. The hardware platform is configured with Intel Core i9-13900K processor, NVIDIA RTX 4090 graphics card and 64 GB memory. The test data used a self-built bimodal data set of parking lot fire, which contained 12480 groups of thermal infrared-visible paired images and 3200 parking lot fire simulation scenes. The annotation categories covered open fire, smoke area, high temperature reflection area and channel occlusion area. In the training phase, brightness perturbation, partial occlusion, view shift and multi-scale cropping are applied to the samples. The data set is divided into training set, validation set and test set according to 7∶2∶1. The experimental parameters are set as follows: the initial learning rate is 0.001, the maximum training round is 240, the batch size is 16, and the input size is set to 160×160 and 320×320, respectively, to check the stability of the method under the conditions of lightweight inference and conventional recognition.

YOLOv5n, Faster R-CNN, Fire-YOLO and the proposed method are selected as comparison methods. The evaluation metrics include precision, recall, F1 score, AUC, and average inference delay, and all results are taken as the mean of 20 repeated experiments with 95% confidence intervals. Fig. 5 shows the recognition accuracy variation of different methods with two input sizes. Fig. 5 (a) corresponds to 160×160 inputs and Fig. 5 (b) corresponds to

320×320 inputs. It can be seen from Fig. 5 that the proposed method still maintains high recognition stability under small-scale input, and the final accuracy reaches 96.84%, which is higher than 93.27% of YOLOv5n, 94.16% of Fire-YOLO, and 90.42% of Faster R-CNN. Under the conventional input size, the accuracy of the proposed method is further improved to 97.84%, and the convergence process is more stable. This indicates that the spatio-temporal adaptive risk coding can effectively suppress the local distortion caused by smoke after the bi-modal feature alignment, and enhance the discriminative response of the flame edge and dangerous hot area.

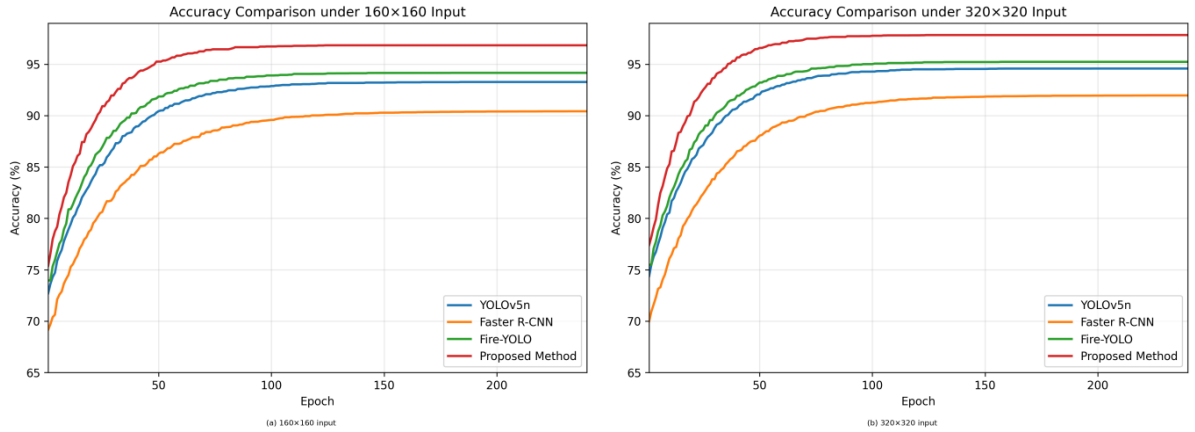


*Figure 5: Accuracy comparison results of different fire target recognition methods*

To further analyze the computational efficiency of the model, Fig. 6 compares the average inference time of each method for two input sizes. Fig.s 6 (a) and 6 (b) correspond to the lightweight input versus the conventional input condition, respectively. The average inference time of the proposed method is 14.7 ms with 160×160 inputs and 34.6 ms with 320×320 inputs, which is slightly higher than that of the pure lightweight model YOLOv5n, but significantly lower than that of Faster R-CNN, while maintaining higher recognition accuracy. This result shows that although the feature reweighting process is added to the risk coding module, the overall reasoning overhead is still within the acceptable range at the robot side.

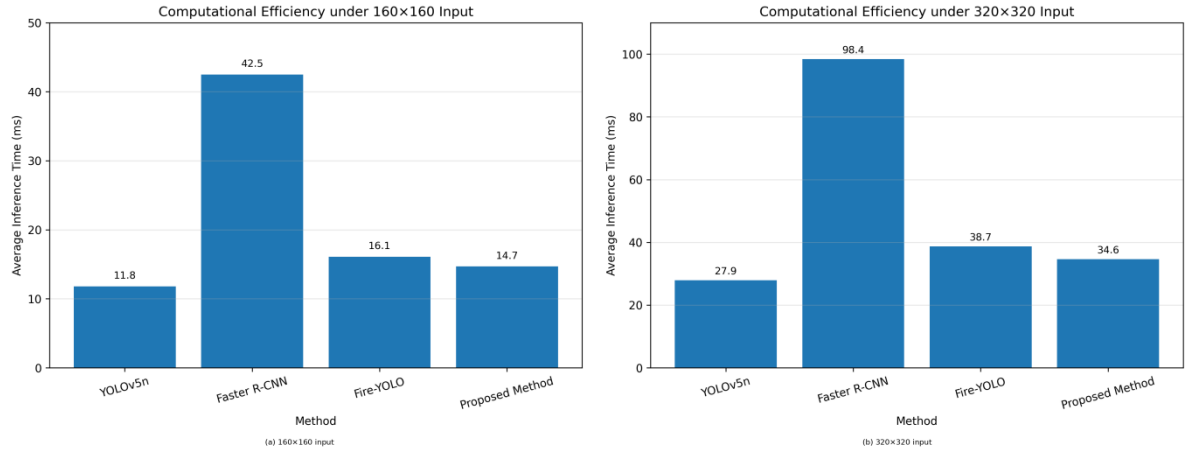


*Figure 6: Comparison results of computational efficiency of different fire target recognition methods*

In order to investigate the generalization performance of the model on different data subsets, Table 2 statistics the main indicators of the proposed method on the training set, validation set and test set.

*Table 2: Recognition performance of the proposed method on different data subsets*

| Data Subset | Accuracy / % | Recall / % | F1 Score | AUC |
|---|---|---|---|---|
| Training Set | 98.25 | 96.43 | 0.9729 | 0.9958 |
| Validation Set | 97.96 | 95.52 | 0.9668 | 0.9947 |
| Test Set | 97.84 | 95.31 | 0.9624 | 0.9939 |

It can be seen that after the fusion of dual-modal features, the spatio-temporal adaptive risk coding not only improves the recognition accuracy of fire targets, but also enhances the usability of the output results for subsequent risk mapping and navigation planning. The classification results show that the recall rate of open fire target is the highest, reaching 97.31%, and the F1 value of smoke target is 0.9516, which indicates that the method has a strong ability to capture fire targets with obvious boundary diffusion and continuous morphological changes. The high temperature reflection area is disturbed by the specular reflection of the metal surface of the car body, and the identification is relatively more difficult. However, under the constraint of risk coding, the false detection rate is still controlled within 2.8%. The above results show that the proposed method can maintain a relatively stable discrimination performance in the parking lot fire environment with low illumination, strong occlusion and non-uniform thermal radiation, and provide a credible fire input for subsequent risk-aware path planning and navigation control.

## 3.2 Performance analysis of risk-aware navigation path planning method

In order to verify the applicability of the risk-aware navigation path planning method in the parking lot fire scene, this study completed the simulation experiment in the joint environment of Gazebo and ROS 2, and repeated the test in the digital twin scene of self-built underground parking lot. The experimental platform is configured with Intel Core i9 processor, RTX 4090 graphics card and 64 GB memory, and the control frequency on the robot side is set to 20 Hz. The scene contains stationary vehicles, randomly opened car doors, collapse obstacles, local high temperature areas and smoke diffusion areas, and the map scale is unified as 80 m×60 m. A*, RRT*, DWA, and Hybrid A* are selected as comparison methods to compare the path length, planning time, replanning times, and collision rate of different algorithms in complex fire environments. All results were averaged over 30 independent experiments and tested for stability with 95% confidence intervals.

As shown in Fig. 7, this paper presents the path planning results of the five methods in a typical parking lot fire scenario. In the figure, the red area represents the high-risk hot area, the gray area represents the smoke occlusion band, and the blue broken line represents the robot planning path. In order to enhance the comparability of the diagram, the average path length and risk exposure index are labeled synchronously next to each path. The average path length of method A is 39.8 m, and the risk exposure index is 0.463. The average path length of RRT method was 45.6 m, and the risk exposure index was 0.358. The average path length of the DWA method is 44.2 m, and the risk exposure index is 0.401. The average path length of Hybrid A method is 43.5 m, and the risk exposure index is 0.296. The average path length of the proposed method is 42.7 m, and the risk exposure index is 0.214. It can be seen that although A is shorter in geometric length, it is easier for A to traverse the local high-risk region. RRT and DWA have obvious path redundancy and local swing in dense obstacle areas. Hybrid A outperforms the previous two in terms of smoothness, but still suffers from insufficient detour

in high smoke areas. The path generated by the proposed method maintains a good balance between length control and risk aversion, which can actively avoid hot area boundaries and low-visibility channels, and maintain a low turning frequency in dense parking areas.

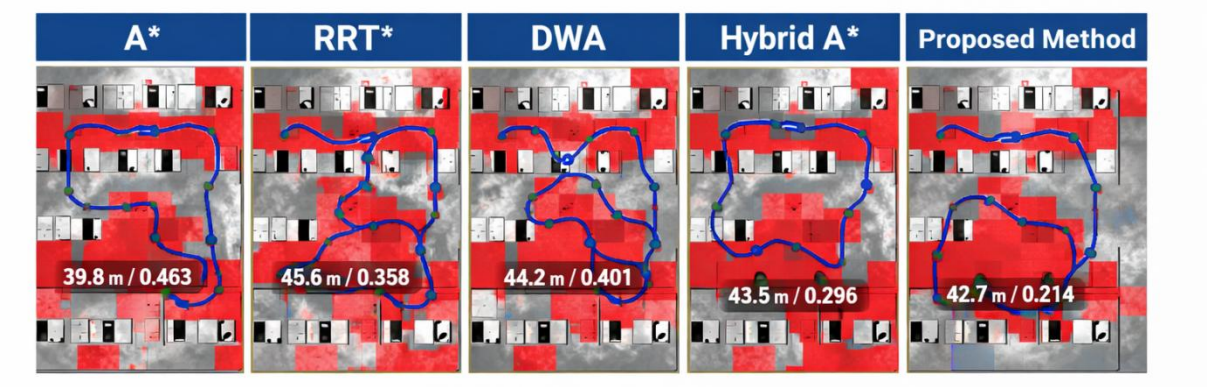


*Figure 7: Comparison of planning results of different path planning methods in a parking lot fire scenario*

To further analyze the differences of each method at the execution level, Table 3 statistics the success rate, minimum safe margin, mean curvature, local replanning recovery delay, and temporal consistency scores of different algorithms on the comprehensive test set. The results show that the task success rate of the proposed method reaches 98.6%, which is higher than that of the other comparison algorithms. The minimum safety distance is 0.81 m, which indicates that it can maintain a larger obstacle avoidance margin during the detour. The mean curvature is controlled at 0.119 $m^{-1}$, indicating that the output path has better smoothness. The recovery delay of local replanning is 0.73 s, and the executable path can still be recovered quickly after the local block in the high-risk area. The time consistency score reaches 0.918, which indicates that the path has good stability maintenance ability under short-term dynamic disturbance conditions.

*Table 3: Comparison of execution performance of different path planning methods*

| Method | Success Rate / % | Minimum Safety Distance / m | Average Curvature / $m^{-1}$ | Local Replanning Recovery Latency / s | Temporal Consistency Score |
|---|---|---|---|---|---|
| A* | 90.7 | 0.62 | 0.184 | 1.26 | 0.781 |
| RRT* | 93.4 | 0.69 | 0.161 | 1.11 | 0.824 |
| DWA | 91.8 | 0.65 | 0.213 | 0.94 | 0.806 |
| Hybrid A* | 95.2 | 0.74 | 0.148 | 0.88 | 0.861 |
| Proposed Method | 98.6 | 0.81 | 0.119 | 0.73 | 0.918 |

It can be seen that the proposed method can better balance path accessibility, local safety and execution continuity in the environment of high occlusion, high disturbance and high risk such as parking lot fire. The risk-aware sampling mechanism reduces the invalid expansion of high-risk areas, the temporal consistency check suppresses the candidate paths that are feasible in a short time but lack of continuity, and the curvature constraint smoothing further reduces the control jitter of differential chassis in narrow channels. Therefore, the proposed method not only maintains good planning quality, but also shows more obvious advantages in execution

stability and scene adaptation, which provides more reliable path input for subsequent navigation decision-making and control strategy.

## 3.3 Performance analysis of navigation decision-making and control strategy of parking lot fire emergency response robot

In order to verify the actual effect of the navigation decision-making and control strategy of the parking lot fire emergency response robot, two types of continuous tasks were set up in the digital twin parking lot. Task A requires the robot to complete the fire source approach, channel reconnaissance and material delivery in turn, and task B requires the robot to complete the smoke area detour, the trapped point arrival and the safe evacuation in turn. The comparison methods include deep reinforcement learning control, rule-driven control and the proposed method. The evaluation metrics are selected as task completion time, global decision entropy, local replanning recovery delay, and number of deadlocks, and all results are averaged over 30 repeated experiments.

As shown in Fig. 8, Fig. 8 (a) shows the global decision entropy of different control strategies in the two types of tasks, and Fig. 8 (b) shows the corresponding average completion time. After iteration stabilization, the global decision entropy of the proposed method on task A and task B is 0.912 and 0.934, respectively, which is significantly lower than 1.086 and 1.124 of deep reinforcement learning control, and lower than 1.203 and 1.271 of rule-driven control. This indicates that after fusing risk state modeling, path consistency assessment, and control allocation correction, the system has lower decision uncertainty under complex fire disturbances. In terms of completion time, the average completion time of the proposed method on task A and task B is 23.4 s and 26.8 s, respectively, which is 4.1 s and 5.3 s shorter than that of the deep reinforcement learning control, and 7.6 s and 8.9 s shorter than that of the rule-driven control.

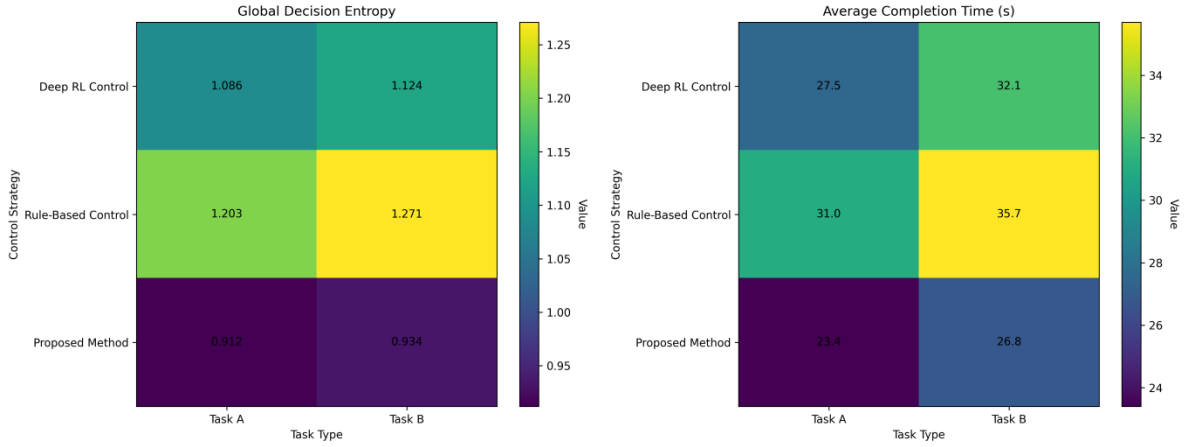


*Figure 8: Performance comparison results of different navigation decisions and control strategies (Figure 8 (a) on the left and Figure 8 (b) on the right)*

Further statistical results show that only one local deadlock occurs in 30 tests, and the proposed method can recover to the executable state within 0.73 s after triggering replanning, and the overall success rate of the task reaches 98.3%. In contrast, deep reinforcement learning control has 3 local deadlocks, and the average recovery delay is 1.21 s. The rule-driven control showed six local deadlocks, and repeated steering and short-term stagnation were more likely to occur in areas with high smoke occlusion. It can be seen that the proposed method can organize the fire recognition results, risk perception path and chassis control instructions into

the same closed-loop link, so that the robot can maintain good decision stability, path tracking continuity and task execution reliability in the parking lot fire environment with high occlusion, high thermal disturbance and dynamic block.

# 4 Discussion

The results in this section show that the robot method for fire emergency response in parking lots constructed in this paper forms a stable computational closed loop at the three levels of recognition, planning and control. In the fire target recognition part, the thermal infrared information, visible light texture and short-term change features are unified into the same representation space through spatio-temporal adaptive risk coding. The recognition accuracy rate is 97.84% and the test set recall rate is 95.31% under 320×320 input, which shows that the method is adaptive to low illumination, strong occlusion and non-uniform thermal radiation conditions. The path planning part does not use the idea of simple shortest path, but combines risk exposure, time consistency and curvature constraints into the cost calculation. Therefore, it not only controls the path length, but also shows stability in the success rate, safety interval, curvature and replanning recovery delay in complex parking scenes. The navigation decision and control layer compresses the recognition results and path output into a unified state link, so that the robot still maintains a lower decision entropy, a shorter completion time and a higher success rate under the conditions of high thermal disturbance and dynamic blocking. Compared with the traditional heuristic methods, the advantage of the proposed method is not the single index extreme value, but the stability formed after the collaboration of multiple modules. This stability comes from three aspects: first, dual-mode fire sensing reduces the impact of single-source input distortion, second, risk-aware sampling and temporal consistency check improve path executability, and third, state transition constraints and control correction mechanism suppress local oscillations in continuous operation. The experimental results also show that the identification, planning or control of robot navigation in the scene cannot be discussed in isolation, and only when environmental risks, motion constraints and decision feedback are put in the same computational framework, the system performance has engineering explanatory power.

# 5 Conclusion

Focusing on the task of parking lot fire emergency response robot, this paper constructs a complete method chain consisting of spatio-temporal scene modeling, fire target recognition, risk-aware path planning, and navigation decision control. Experimental results show that the proposed method has achieved good performance in terms of dual-modal fire recognition accuracy, path safety and control stability, and can provide computational support for autonomous reconnaissance and response in closed fire environments. At the same time, this paper still has some limitations. The data set mainly comes from self-built simulation scenes and controlled samples, and the coverage of extreme smoke, continuous dedetonation and multi-robot cooperation conditions is not sufficient. The risk weights and state transition parameters still depend on the offline setting, and the online adaptive ability still has room to be further enhanced. At present, the control verification is mainly based on digital twin and hardware-in-the-loop environment. More systematic tests are needed for communication occlusion, ground wetness and sensing drift in real parking lots. Future research will be carried out for lightweight deployment, online parameter self-updating, multi-robot cooperative rescue and cross-scenario migration, to further improve the generalization ability, robustness and real-

time execution ability of the system in real fire environment. At the method level, causal risk modeling, event-driven replanning and multimodal uncertainty estimation can be further introduced into the unified framework, so as to form a tighter data closed loop between identification output, path update and control execution, and improve the response accuracy of the system to sudden heat source migration, local collapse and evacuation flow disturbance. At the same time, it is necessary to carry out long-term operation verification combined with edge computing platform to further evaluate the continuous stability, real-time response ability and field deployment reliability of the model under resource-constrained conditions.

# References

[1] Wu B, Chi X, Zhao C, et al. Dynamic path planning for forklift AGV based on smoothing A* and improved DWA hybrid algorithm[J]. Sensors, 2022, 22(18): 7079.

[2] Yang H, Teng X. Mobile robot path planning based on enhanced dynamic window approach and improved A∗ algorithm[J]. Journal of robotics, 2022, 2022(1): 2183229.

[3] Chen Y, Cheng C, Zhang Y, et al. A neural network-based navigation approach for autonomous mobile robot systems[J]. Applied Sciences, 2022, 12(15): 7796.

[4] Sathiya V, Chinnadurai M, Ramabalan S. Mobile robot path planning using fuzzy enhanced improved multi-objective particle swarm optimization (FIMOPSO)[J]. Expert systems with applications, 2022, 198: 116875.

[5] Chen Z, Wu H, Chen Y, et al. Patrol robot path planning in nuclear power plant using an interval multi-objective particle swarm optimization algorithm[J]. Applied soft computing, 2022, 116: 108192.

[6] Jiang Z, Wang W, Sun W, et al. Path planning method for mobile robot based on a hybrid algorithm[J]. Journal of Intelligent & Robotic Systems, 2023, 109(3): 47.

[7] Liu C, Xie S, Sui X, et al. PRM-D* method for mobile robot path planning[J]. Sensors, 2023, 23(7): 3512.

[8] Hao K, Yang Y, Li Z, et al. CERRT: a mobile robot path planning algorithm based on RRT in complex environments[J]. Applied Sciences, 2023, 13(17): 9666.

[9] Bulut V. Path planning of mobile robots in dynamic environment based on analytic geometry and cubic Bézier curve with three shape parameters[J]. Expert Systems with Applications, 2023, 233: 120942.

[10] Zhang Y, Chen P. Path planning of a mobile robot for a dynamic indoor environment based on an sac-lstm algorithm[J]. Sensors, 2023, 23(24): 9802.

[11] Tan J. A method to plan the path of a robot utilizing deep reinforcement learning and multi-sensory information fusion[J]. Applied Artificial Intelligence, 2023, 37(1): 2224996.

[12] Li X, Wang L, An Y, et al. Dynamic path planning of mobile robots using adaptive dynamic programming[J]. Expert Systems with Applications, 2024, 235: 121112.

[13] Wang J, Han H, Han X, et al. Reinforcement learning path planning method incorporating multi-step Hindsight Experience Replay for lightweight robots[J]. Displays, 2024, 84: 102796.

[14] Xiao H, Chen C, Zhang G, et al. Reinforcement learning-driven dynamic obstacle avoidance for mobile robot trajectory tracking[J]. Knowledge-Based Systems, 2024, 297: 111974.

[15] Tao B, Kim J H. Deep reinforcement learning-based local path planning in dynamic environments for mobile robot[J]. Journal of King Saud University-Computer and Information Sciences, 2024, 36(10): 102254.

[16] Liu S, Tian Q, Tang C. Mobile robot path planning algorithm based on NSGA-II[J]. Applied Sciences, 2024, 14(10): 4305.

[17] Wang J, Zheng E. Path planning of a mobile robot based on the improved rapidly exploring random trees star algorithm[J]. Electronics, 2024, 13(12): 2340.

[18] Dang T V, Tan P X. Hybrid mobile robot path planning using safe JBS-A* B algorithm and improved DWA based on monocular camera[J]. Journal of Intelligent & Robotic Systems, 2024, 110(4): 151.

[19] Mukhiddinov M, Abdusalomov A B, Cho J. A wildfire smoke detection system using unmanned aerial vehicle images based on the optimized YOLOv5[J]. Sensors, 2022, 22(23): 9384.

[20] Lu K, Xu R, Li J, et al. A vision-based detection and spatial localization scheme for forest fire inspection from UAV[J]. Forests, 2022, 13(3): 383.

[21] Wang Z, Wu L, Li T, et al. A smoke detection model based on improved YOLOv5[J]. Mathematics, 2022, 10(7): 1190.

[22] Shahid M, Virtusio J J, Wu Y H, et al. Spatio-temporal self-attention network for fire detection and segmentation in video surveillance[J]. Ieee Access, 2021, 10: 1259-1275.

[23] Kim S Y, Muminov A. Forest fire smoke detection based on deep learning approaches and unmanned aerial vehicle images[J]. Sensors, 2023, 23(12): 5702.